Towards a consistent model for both the Hi and stellar mass functions of galaxies

Article (Published Version)

Monthly Notices
of the
ROYAL ASTRONOMICAL SOCIETY

MNRAS **472,** 1981–1990 (2017)
Advance Access publication 2017 August 18

doi:10.1093/mnras/stx2131

Towards a consistent model for both the H I and stellar mass functions of galaxies

Hazel Martindale,[1⋆] Peter A. Thomas,[1⋆] Bruno M. Henriques[2,3] and Jon Loveday[1]

[1]*Astronomy Centre, University of Sussex, Falmer, Brighton BN1 9QH, UK*
[2]*Max-Planck-Institut für Astrophysik, Karl-Schwarzschild-Str. 1, 85741 Garching b. München, Germany*
[3]*Institute for Astronomy, ETH Zurich, CH-8093 Zurich, Switzerland*

Accepted 2017 August 15. Received 2017 August 14; in original form 2016 June 25

ABSTRACT

Using the L-Galaxies semi-analytic model we simultaneously fit the H I mass function, stellar mass function and the fraction of red galaxies. We find good fits to all three observations at $z = 0$ and to the stellar mass function and red fraction at $z = 2$. Using Markov Chain Monte Carlo (MCMC) techniques we adjust the L-Galaxies parameters to best fit the constraining data. In order to fit the H I mass function we must greatly reduce the gas surface density threshold for star formation, thus lowering the number of low H I mass galaxies. A simultaneous reduction in the star formation efficiency prevents the overproduction of stellar content. A *simplified* model in which the surface density threshold is eliminated altogether also provides a good fit to the data. Unfortunately, these changes weaken the fit to the Kennicutt–Schmidt relation and raise the star formation rate density at recent times, suggesting that a change to the model is required to prevent accumulation of gas on to dwarf galaxies in the local Universe.

Key words: methods: numerical – galaxies: evolution – galaxies: formation.

1 INTRODUCTION

Cold gas provides the fuel for star formation and understanding its properties in galaxies is fundamental to a complete model of galaxy formation. While the physics governing the collapse of gas clouds on sub-pc scales, and its subsequent conversion into stars, remain largely unknown, simulations can be used to explore the factors that affect the gas and ultimately the stellar content of galaxies.

The relations governing star formation link the cold gas content to the amount of stars formed. The widely used Kennicutt–Schmidt relation (Schmidt 1959; Kennicutt 1998) is a relation between total cold gas surface density content and the star formation rate surface density of a galaxy. More recent observations, however, have shown the correlation to be stronger with only the molecular, H_2 component of cold gas (Bigiel et al. 2008; Leroy et al. 2008).

H_2 gas is not directly detected and is instead observed via a tracer such as the CO molecule which adds uncertainty to these measurements. The H I component, on the other hand, correlates more weakly with star formation than the H_2 , but can be directly observed through the 21 cm emission. H I surveys such as the H I Parkes All-Sky Survey (HIPASS; Meyer et al. 2004) and the Arecibo Legacy Fast ALFA survey (ALFALFA; Giovanelli et al. 2005) now provide large samples of statistical significance. The H I mass function from these surveys measures masses down to 10^6 $M_\odot$ allowing galaxy gas content to be probed across a full range of masses (Zwaan et al. 2005; Martin et al. 2010). Up coming surveys at new facilities such as the Australian SKA pathfinder (ASKAP; Johnston et al. 2008), Karoo Array Telescope (MeerKAT; Booth et al. 2009) and the Square Kilometre Array (SKA[1]) will greatly improve the observational constraints on H I content of galaxies. For that reason, we choose to use H I as a constraint in our models.

Semi-analytic models (SAMs) provide a framework to explore the statistical properties of the observed galaxy population. The evolution of large-scale structures is given by dark matter merger trees, either from *N*-body simulations or analytic calculations, and the baryonic component is modelled via empirical relations that are designed to capture the key physics (White 1988; Cole 1991; Lacey & Silk 1991; White & Frenk 1991; Kauffmann, White & Guiderdoni 1993; Kauffmann 1999; Somerville & Primack 1999; Springel et al. 2001; Hatton et al. 2003; Kang et al. 2005; Croton et al. 2006; De Lucia & Blaizot 2007; Guo et al. 2011; Lu et al. 2011; Benson 2012). A downside of SAMs is that they necessarily impose restrictive assumptions about the geometry of galaxies and the exchange of material with their surroundings. The major advantage over hydrodynamical simulations is that they are quick to run allowing us to explore the impact of different implementations of physical processes and different parameter values. In recent years, the introduction of robust statistical methods has even allowed the full exploration of parameter space (Kampakoglou, Trotta & Silk 2008; Henriques et al. 2009; Benson & Bower 2010; Bower et al. 2010;

⋆ E-mail: hrmartindale@gmail.com (HM); p.a.thomas@sussex.ac.uk (PAT)

[1] https://www.skatelescope.org/project/

Henriques & Thomas 2010; Lu et al. 2011, 2012; Mutch, Poole & Croton 2013; Henriques et al. 2013; Benson 2014; Ruiz et al. 2015).

The most recent version of the L-Galaxies SAM (Henriques et al. 2015, hereafter HWT15) provides an excellent fit to a wide range of galaxy properties across a wide range of redshifts. In this paper, we aim to improve the agreement between the HWT15 model to the H I mass function by including it as an extra constraint in addition to the stellar mass function and galaxy red fraction. We find that we can obtain a good fit to all data sets simultaneously by lowering, or even eliminating altogether, the surface density threshold for star formation. Unfortunately, these changes weaken the fit to the Kennicutt–Schmidt relation and raise the star formation rate density (SFRD) at recent times, suggesting that a change in the model is required to prevent accumulation of gas on to dwarf galaxies in the local Universe.

The paper is structured as follows: In Section 2, we describe the L-Galaxies semi-analytic model and the method of gas division. In Section 3, we present the results of constraining the model with the H I mass function in addition to the galaxy red fraction and stellar mass function. In Section 4, we examine which parameters have changed in order to produce a good fit to all constraining data sets and compare our results to the Kennicutt–Schmidt relation. We provide our conclusions in Section 5.

2 METHOD

2.1 L-Galaxies

Semi-analytic models provide a tool to explore galaxy formation and evolution and simulate the cosmic galaxy population. The models use coupled differential equations to follow the evolution of the baryonic component of galaxies usually constructed on top of dark matter haloes from an *N*-body simulation. Many aspects of galaxy formation are included in these models such as, star formation, gas cooling, metal enrichment, black hole growth and feedback processes.

The Munich SAM, L-Galaxies, has been developed over many years using galaxy formation recipes to match the observed galaxy populations (White 1988; Kauffmann et al. 1993; Kauffmann 1999; Springel et al. 2001, 2005; Croton et al. 2006; De Lucia & Blaizot 2007; Guo et al. 2011, 2013; Henriques et al. 2013; Henriques et al. 2015). The underlying merger trees are extracted from the Millennium (Springel et al. 2005) and MillenniumII Simulations (Boylan-Kolchin et al. 2009). The latest version of the model, on which this work is based, is given in HWT15. This version uses *Planck* year 1 cosmology with the Millennium dark matter merger trees scaled according to the method of Angulo & White (2010) (as updated by Angulo & Hilbert 2015). HWT15 constrain the model to give a good fit to the stellar mass function and the fraction of red galaxies over the redshift range 0–3. A full description of the model is given in the supplementary material of HWT15.

2.1.1 MCMC

Having many recipes controlling galaxy formation gives rise to numerous free parameters which, when considering individual galaxy properties independently, are frequently degenerate with each other. It would be a long and inefficient process of trial and error to adjust the parameters to best fit the observations by hand when alterations to the model are made. We employ the MCMC procedure within L-Galaxies to find a best fit set of parameters (Henriques et al. 2009; Henriques et al. 2013). This method approximates a likelihood value for the ability of the model to recover the observed galaxy property and then uses the MCMC technique to minimize that value and locate a best set of parameters.

2.1.2 Star formation law

In the model we assume stars form from the total cold gas within a given galaxy's disc (i.e. the model does not distinguish between H I and molecular gas). The star formation rate is given by

$$\dot{M}_{\rm stellar} = \alpha_{\rm SF} \frac{\left(M_{\rm gas} - M_{\rm crit}\right)}{t_{\rm dyn,disc}}, \tag{1}$$

where $\alpha_{\rm SF}$ is a normalization parameter, $M_{\rm gas}$ is the total cold gas mass, $t_{\rm dyn,disc}$ is the dynamical time, and $M_{\rm crit}$ is a threshold mass whose need is based on a historical assumption that there is a minimum surface density required for star formation (Kauffmann 1996; Kennicutt 1998). Based on the argument in Kauffmann (1996) we take $M_{\rm crit}$ to have the form

$$M_{\rm crit} = M_{\rm crit,0} \left(\frac{V_{\rm 200c}}{200\ {\rm km\ s^{-1}}}\right) \left(\frac{R_{\rm gas}}{10\ {\rm kpc}}\right), \tag{2}$$

where $V_{\rm 200c}$ is the virial speed of the halo, $R_{\rm gas}$ is the gas disc scale-length, and $M_{\rm crit,\,0}$ is a normalization constant. Since Kauffmann (1999) and prior to HWT15, all versions of the Munich model fixed $M_{\rm crit,0} = 3.8 \times 10^9\ {\rm M}_\odot$. However, observations now indicate that star formation is linked more closely to the molecular gas than to the total gas content (Bigiel et al. 2008; Leroy et al. 2008). Ideally the critical mass threshold should arise out of the model rather than being imposed and future versions of the L-Galaxies model will follow H_2 explicitly in order to explore this possibility. Until then (from HWT15 onwards) we treat $M_{\rm crit,\,0}$ as a free parameter.

2.2 The H I model

We use the model of Blitz & Rosolowsky (2006, hereafter BR06) to divide the cold gas into its H I and H_2 components in post-processing. In this model, the ratio of H I to H_2 gas in a galaxy is determined by mid-plane hydrostatic pressure in the galactic disc. Elmegreen (1989, 1993) propose a form for the mid-plane pressure

$$P_{\rm ext} \approx \frac{\pi}{2} G \Sigma_{\rm gas} \left(\Sigma_{\rm gas} + \Sigma_{\rm star} \frac{c_{\rm gas}}{c_{\rm star}}\right), \tag{3}$$

where $\Sigma_{\rm gas}$, $\Sigma_{\rm star}$ are the cold gas and stellar surface densities, $c_{\rm gas}$, $c_{\rm star}$ are the gas and stellar vertical velocity dispersions and G is the gravitational constant. The mid-plane pressure is calculated from the equations of hydrostatic equilibrium for a thin disc of gas and stars. This pressure is an important factor in the formation of giant clouds within which H_2 is found. BR06 make the assumption that the ratio of H_2 to H I in the galaxy is a function of the pressure given in (3). The relation takes the form of a power law:

$$R_{\rm mol} = \frac{\Sigma_{\rm H2}}{\Sigma_{\rm H\,I}} = \left(\frac{P_{\rm ext}}{P_0}\right)^{\alpha}, \tag{4}$$

where $\Sigma_{\rm H2}$ and $\Sigma_{\rm HI}$ are the disc surface densities of H_2 and H I gas, respectively and P_0 and α are fitting constants. This was further explored using resolved observations of galaxies (Blitz & Rosolowsky 2006; Leroy et al. 2008).

This model of gas division requires information on the radial distribution of gas inside galaxies. In order to include it at each step of the L-Galaxies MCMC chain without prohibitively slowing the

calculation we use the approximation to BR06 model derived in Obreschkow et al. (2009, hereafter O09). They write $R_{\rm mol}$ as,

$$R_{\rm mol} = R^{c}_{\rm mol} \exp(-1.6\, r/r_{\rm disc}), \quad (5)$$

where $r_{\rm disc}$ is the scalelength of the gas disc and $R^{c}_{\rm mol}$ is

$$R^{c}_{\rm mol} = \left[K r^{-4}_{\rm disc} M_{\rm gas}(M_{\rm gas} + \langle f_\sigma \rangle\, M^{\rm stars}_{\rm disc})\right]^{\alpha}, \quad (6)$$

where $M_{\rm gas}$ is the total cold gas mass, $M^{\rm stars}_{\rm disc}$ is the mass of the stellar disc and $K = G/(8\pi P_0)$. We adopt the same values of constants as O09: $P_0 = 2.34 \times 10^{-13} Pa$, $\alpha = 0.8$ and $\langle f_\sigma \rangle = 0.4$ which is the ratio of the velocity dispersions in equation (3) taken from observations of Elmegreen (1993). Through $R_{\rm mol}$ we can derive expressions for the surface density of H I and H_2 which when integrated give the $M_{\rm H\,I}$ and $M_{\rm H2}$.

O09 approximate the integration, finding that the ratio of H_2 to H I is given by

$$\frac{M_{\rm H2}}{M_{\rm H\,I}} = \frac{\int \Sigma_{\rm H2}(r)\ {\rm d}A}{\int \Sigma_{\rm H\,I}(r)\, {\rm d}A} \approx \left(3.44 R^{c\ -0.506}_{\rm mol} + 4.82 R^{c\ -1.054}_{\rm mol}\right)^{-1}. \quad (7)$$

Using this approximation along with assuming that $M_{\rm H} = M_{\rm H\,I} + M_{\rm H\,II}$ we can calculate the masses without dividing the galaxies into rings and significantly speed up the calculation. We assume that $M_{\rm H} = 0.74 M_{\rm coldgas}$. In agreement with O09 we find that the approximate value is within 2 per cent of that from the full calculation for ∼95 per cent of our galaxies.

2.3 Observational constraints

We constrain the model using observations at $z = 0$ and $z = 2$. At $z = 0$ we use:

(i) The stellar mass function is a combination of the SDSS (Li & White 2009) and GAMA (Baldry et al. 2012) results.

(ii) The H I mass function is a combination from HIPASS (Zwaan et al. 2005) and ALFALFA (Haynes et al. 2011). The combination of these data sets is shown in Appendix B below.

(iii) The red fraction is obtained by dividing the stellar mass function of red galaxies by the sum of the red and blue stellar mass functions. We use data from Bell et al. (2003) and Baldry et al. (2012).

At $z = 2$:

(i) The stellar mass function is a combination of COSMOS (Domínguez Sánchez et al. 2011), ULTRAVISTA (Ilbert et al. 2013; Muzzin et al. 2013) and ZFOURGE (Tomczak et al. 2014).

(ii) The red fraction of galaxies also uses COSMOS (Domínguez Sánchez et al. 2011), ULTRAVISTA (Ilbert et al. 2013; Muzzin et al. 2013) and ZFOURGE (Tomczak et al. 2014).

When we use these observational constraints from different surveys they are combined into just one value. This is done by averaging the values within each mass bin together. The 1σ errors on these values are then taken to be half the minimum to maximum range. Further details of this process are described in appendix 2 of HWT15.

3 RESULTS

We present results for several different versions of the model:

(i) HWT15 (green dash–dotted line): The reference model, which did not use the H IMF as a constraint.

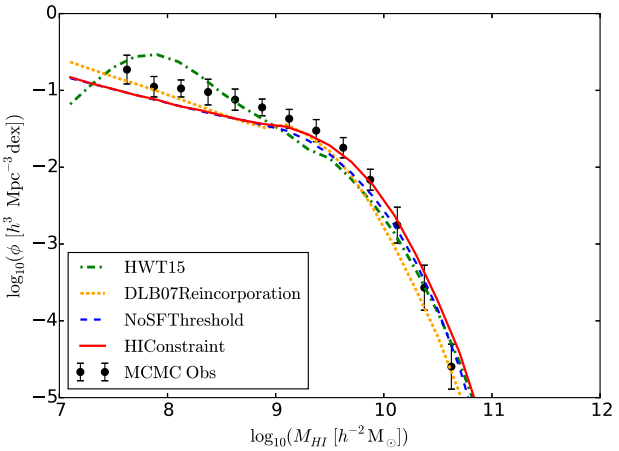

Figure 1. The H I mass function at $z = 0$. The black points are the observed H I mass function from HIPASS. The coloured lines represent the different models: green, HWT15; red, HIConstraint; blue, NoSFThreshold; yellow, DLB07 Reincorporation.

(ii) HIConstraint (red solid line): The HWT15 model but adding in the H IMF as a constraint at $z = 0$.

(iii) NoSFThreshold (blue dashed line): The same as the HIConstraint but with the minimum threshold surface density for star formation set equal to zero.

(iv) DLB07 Reincorporation (yellow dotted line): As for the HIConstraint but using the older (De Lucia & Blaizot 2007, hereafter DLB07) recipe for reincorporation of ejected material.

All of the the models were constrained to simultaneously match the observations described in Section 2.3, except HWT15 which did not use the H IMF as a constraint.

3.1 H I mass function

The H I mass function is shown in Fig. 1. It is immediately obvious that the HWT15 reference model is a poor fit to observations. This is not an inherent deficiency of the model, but results from the fact that the observed mass function was not used as an input constraint. The HWT15 model does, in fact, provide a slightly better fit overall to the stellar masses and galaxy colours at $z = 0$ and 2, than the HIConstraint or NoSFThreshold model, but the difference is slight. That goes to show that the H I mass function serves as a largely independent constraint.

The HIConstraint model, however, that does use the H I as an additional constraint, provides a very good fit to the H I mass function. It does that largely by reducing the $\Sigma_{\rm SF}$ parameter in the model that governs the minimum surface density for quiescent star formation (see Table 1). This allows more cold gas to be consumed in low-mass galaxies. In order to maintain the same overall stellar mass, the star formation efficiency is reduced leading to a reduction of gas consumption in high-mass galaxies.

Because the HIConstraint model lowers the minimum surface density for star formation so much, we also examined a NoSFThreshold model in which it is set equal to zero (thus reducing the number of free parameters in the model by one). The two are barely distinguishable in their predictions (except that the NoSFThreshold model has slightly bluer colours – see Section 3.3).

To try to understand why Lu et al. (2014, hereafter Lu14) have claimed that it is not possible to reproduce the H I mass function, we also ran a model that is identical in every respect to the

Table 1. Parameters constrained by the MCMC model. Best-fitting parameters are given for each model as well as HWT15 for comparison.

Parameter	HWT15	HIConstraint	NoSFThreshold	DLB07 Reincorporation	Units
$\alpha_{\rm SF}$ (SF eff)	0.025	0.010	0.0099	0.0030	
$\Sigma_{\rm SF}$ (SF gas density threshold)	0.24	0.0042	1e-6	0.0079	$10^{10}\,{\rm M}_\odot\,{\rm pc}^{-2}$
$\alpha_{\rm SF,\,burst}$ (SF Burst eff)	0.60	0.89	0.43	0.82	
$\beta_{\rm SF,\,burst}$ (SF Burst Slope)	1.9	1.7	0.97	1.61	
$k_{\rm AGN}$ (Radio feedback eff)	0.0053	0.014	0.039	7.1×10^{-4}	${\rm M}_\odot\,{\rm yr}^{-1}$
$f_{\rm BH}$ (Black hole growth eff)	0.041	0.025	0.026	0.040	
$V_{\rm BH}$ (Quasar growth scale)	750	552	953	630	${\rm km\,s}^{-1}$
ϵ (Mass-loading eff)	2.60	1.3	1.5	1.5	
$V_{\rm reheat}$ (Mass-loading scale)	480	338	341	136	${\rm km\,s}^{-1}$
β_1 (Mass-loading slope)	0.72	1.11	0.32	3.5	
η (SN ejection eff)	0.62	0.30	0.58	0.28	
$V_{\rm eject}$ (SN ejection scale)	100	184	138	131	${\rm km\,s}^{-1}$
β_2 (SN ejection Slope)	0.80	2.4	4.4	3.1	
γ (Ejecta reincorporation)	3.0×10^{10}	1.3×10^{10}	1.7×10^{10}	0.13	yr
y (Metal yield)	0.046	0.028	0.021	0.019	
$R_{\rm merger}$ (Major-merger threshold)	0.10	0.10	0.10	0.10	
$\alpha_{\rm friction}$ (Dynamical friction)	2.5	2.6	2.9	1.2	
$M_{\rm r.p.}$ (Ram-pressure threshold)	1.2×10^4	3.0×10^4	1.7×10^4	1.2	$10^{10}\,{\rm M}_\odot$

HIConstraint model, except that the reincorporation time-scale follows the parametrization given in DLB07 rather than HWT15. This DLB07 model, which uses H I as a constraint, provides a better fit than the original HWT15 but is clearly significantly worse than either the HIConstraint or NoSFThreshold models. This will be discussed further in Section 4.4 below.

3.2 Stellar mass function

The stellar mass function is shown in Fig. 2, the upper panel showing $z = 0$ and the lower $z = 2$. At $z = 0$ we find an excellent fit to the observed stellar mass function in both the HIConstraint and NoSFThreshold models, very similar to that of the reference model of HWT15. There is no significant difference between the red and blue lines indicating that a non-zero threshold cold gas surface density is not required to fit the stellar mass function at $z = 0$. The DLB07 reincorporation model provides a significantly worse fit both at the knee of the SMF and the slope at low-masses. This is discussed further in Section 4.4.

The fit at $z = 2$ is worse than in HWT15 for both our models. Below the knee of the distribution all models are very similar but, above the knee, the HIConstraint and NoSFThreshold models have fewer high stellar mass galaxies than the observations or HWT15 (note, however, that the observations have large uncertainties in this region). The DLB07 reincorporation model again fares worse than the others.

3.3 Fraction of red galaxies

The model was also constrained using the red fraction of galaxies, with the same prescription as described in Section 4.2 of HWT15. That paper used the distribution of model galaxies in the $u - r$ versus M_r plane to divide the galaxies into an active, blue, and a passive, red population at $z = 0$ and the $U{-}V$ versus $V{-}J$ colour plane at higher redshifts. The same observables are used to select model galaxies as in observational studies but we adjust the placement of the dividing line between red and blue galaxies to correctly separate

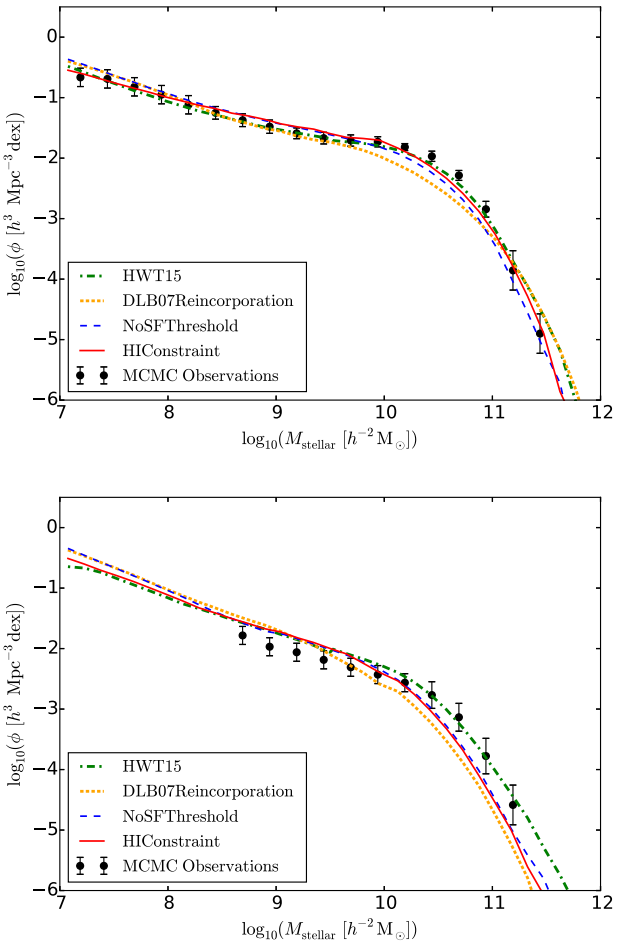

Figure 2. The stellar mass function, $z = 0$ is shown in the upper panel and $z = 2$ is shown in the bottom panel. The black points are the observations used within the MCMC as constraints. The coloured lines are as in Fig. 1.

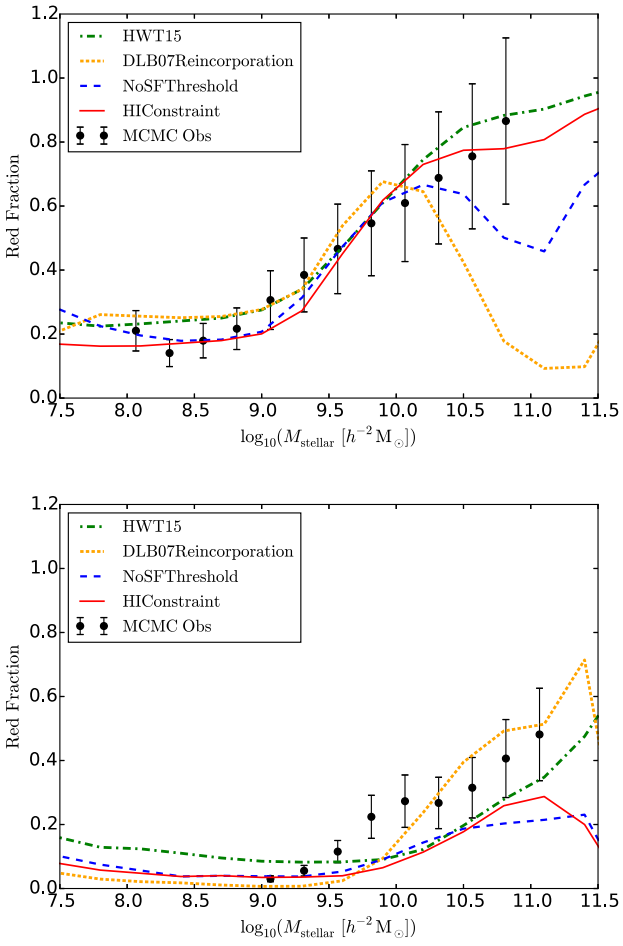

Figure 3. The red fraction mass function shown in the upper panel is $z = 0$, and $z = 2$ is shown in the lower. The line colours refer to the same models as those in Fig. 2. The black points are the observed red fractions used within the MCMC.

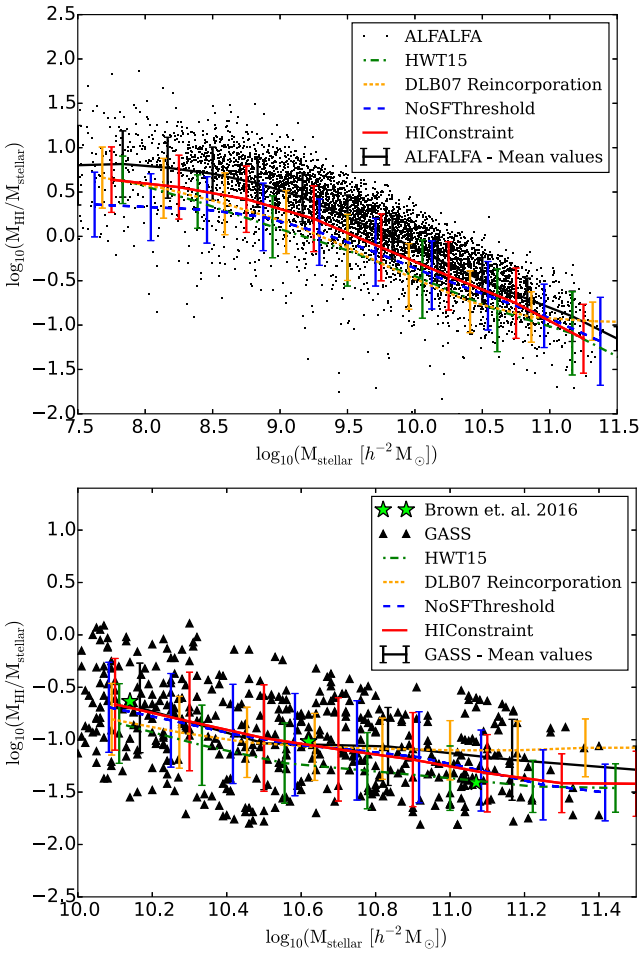

Figure 4. The H I to stellar mass fraction as a function of stellar mass. The top panel compares our data to that from the ALFALFA survey, (Haynes et al. 2011). The lower panel compares with the GASS survey, triangles, (Catinella et al. 2013) and Brown et al. (2015), green stars. We show the mean gas fraction in bins of stellar mass as coloured lines, the colours are as previously. The upper error bar values show the 84th percentile in that stellar mass bin while the lower show the 16th percentile. For comparison as a black line we show the means and percentiles of the ALFALFA, upper panel, and GASS, lower panel, surveys.

the two populations in the model. This allows for a direct comparison between the relative numbers of galaxies in each population independently of any differences on the global colour distributions arising from systematics in the stellar population synthesis or dust modelling. The red fraction is shown in Fig. 3 with $z = 0$ in the upper panel and $z = 2$ in the lower panel.

At $z = 0$ the HIConstraint model matches the data best, with the HWT15 and the DLB07 Reincorporation models having slightly too many passive galaxies at low mass, and the NoSFThreshold and DLB07 Reincorporation models having too many active galaxies at high mass.

At $z = 2$, all but the DLB07 Reincorporaton model underpredict the fraction of red galaxies at high stellar mass. The decrease in the red population at $z = 2$ indicates the model has too much ongoing star formation in the highest mass galaxies. This suggests that the reduction of the threshold for star formation may not be an ideal solution to our problem, as discussed further in Section 4.2, below.

3.4 Gas fractions

We calculate the H I to stellar mass ratio and compare it to those observed by the ALFALFA (Haynes et al. 2011) and Galex Arecibo SDSS Survey (GASS) (Catinella et al. 2013) surveys. In general we have good agreement with the observed H I gas fractions shown in Fig. 4. The top panel of Fig. 4 compares the models to ALFALFA while the bottom compares to GASS. The contour levels shown in Fig. 4 for each model enclose 68, 90 and 99 per cent of the data.

The ALFALFA survey is a flux limited survey and due to the survey selection it cannot observe very low H I mass galaxies. This leads to the survey preferentially observing high H I flux spiral galaxies and missing low H I flux objects with correspondingly low gas fractions. In order to perform a detailed comparison we would need to precisely mimic the survey selection of ALFALFA in model galaxies. In this work when we compare to ALFALFA we perform a crude selection on the semi-analytic galaxies, converting the H I mass to a H I flux by setting an observer at the centre of the simulation box. We also project a velocity width for the model galaxies and this is also used according to the ALFALFA selection function. This selection has been applied to the model galaxies in the top panel of Fig. 4. These then span the similar range of stellar mass as the ALFALFA data.

In the lower panel of Fig. 4 we compare our model results to the GASS survey for which the galaxies are stellar mass selected and

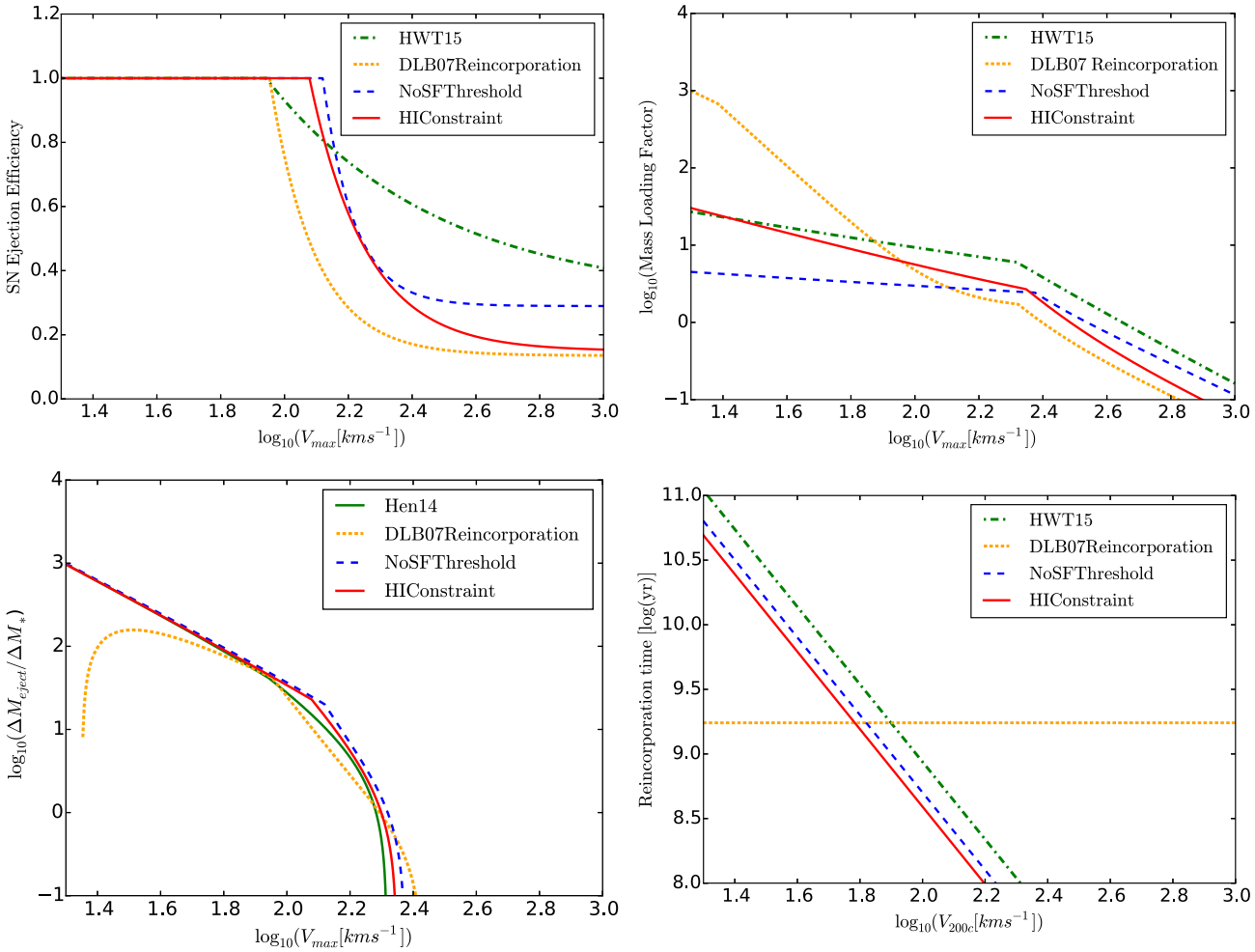

Figure 5. Supernova feedback parameters as functions of the halo velocity either maximum circular velocity, $V_{\rm max}$ or virial velocity V_{200c}. Top left is the SN Ejection Efficiency: the fraction of available SN energy for use in gas reheating and ejection. Top right is the Mass-loading Efficiency, that controls how much cold gas is reheated. Bottom left shows a derived quantity, the ratio of the mass of hot ejected gas to cold gas mass turned into stars. Finally, bottom right shows the Reincorporation Time-scale for ejected gas. In all plots the colours represent the same models as described above. All plots are at $z = 0$.

span more fully the complete range of gas fractions. As with the ALFALFA above we have cut the model galaxies to reproduce the survey. Here, theoretical predictions match the observed gas fractions reasonably well. The different distribution of galaxy masses, particularly obvious at high stellar mass, arises because the GASS survey is not volume-limited. We have also included on this figure data from Brown et al. (2015). This data set stacks detections and non-detections from the GASS and ALFALFA surveys. The resulting average gas fraction points agree well with the model data, passing through the middle of the contours.

4 DISCUSSION

4.1 Changes to model parameters

We start our discussion with the original HWT15 model and the new HIConstraint and NoSFThreshold models. We defer the discussion of the DLB07 model to the final paragraph of this section and Section 4.4.

The best-fitting parameters for our models are shown in Table 1. When adding in the H I mass function constraint into the HIConstraint and NoSFThreshold models several parameters have changed significantly from those of the original HWT15 model. The biggest change is to the surface density threshold for star formation, $M_{\rm crit,\,0}$, that we imposed. As described in Section 2.1.2 we have freed further the threshold parameter to allow it to become very low, or have forced its removal entirely, to allow a reduction in the H I content of low-mass galaxies. As compensation the star formation efficiency has decreased, preventing the overproduction of stars in more massive systems. The parameters controlling the feedback processes have changed slightly compared to HWT15. In Fig. 5, we plot the formulae that control feedback as a function of virial velocity. These formulae can be found in the supplementary material of HWT15.

The top-left panel of Fig. 5 shows that the new models prefer a sharp reduction in SN ejection efficiency above a halo circular speed of about 100 km s^{-1}, dropping to just 10–20 per cent at higher masses. This allows more retention of gas in high-mass systems. Slightly unexpectedly, the mass-loading factors, shown in the top-right panel of the figure, are lower than for the fiducial HWT15 model, except for DLB07 Reincorporation that requires large mass-loading in dwarf galaxies to offset the rapid reincorporation (and subsequent cooling) of ejected gas (bottom-right panel). Unfortunately for that model, the expenditure of energy to heat extra cold gas results in a decrease of mass ejected in those dwarfs for a given

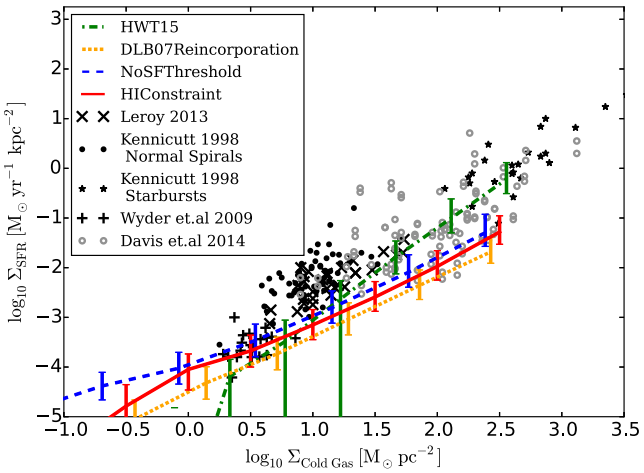

Figure 6. Relationship between total gas surface density and the star formation rate surface density. The colours represent the same four models as previously and the lines are as described in Fig. 4 showing the mean and percentile range in bins of stellar mass. The black data points represent observed values from four different studies (Kennicutt 1998; Wyder et al. 2009; Leroy et al. 2013; Davis et al. 2014).

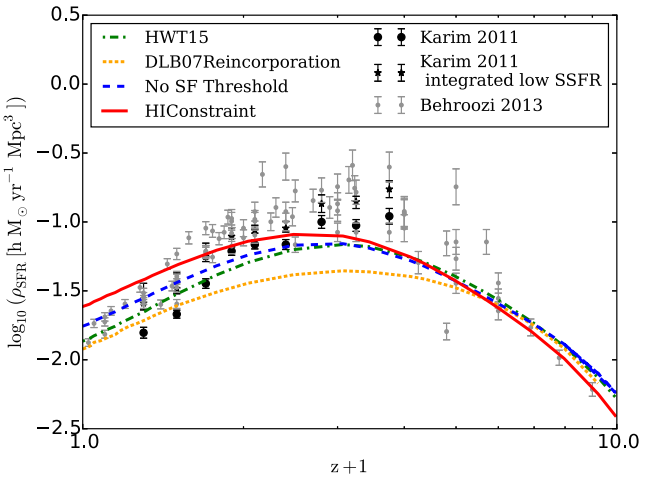

Figure 7. The cosmic SFRD. The colours again represent the four models. These are compared to observations with the black data points from Karim et al. (2011) and the grey from Behroozi, Wechsler & Conroy (2013).

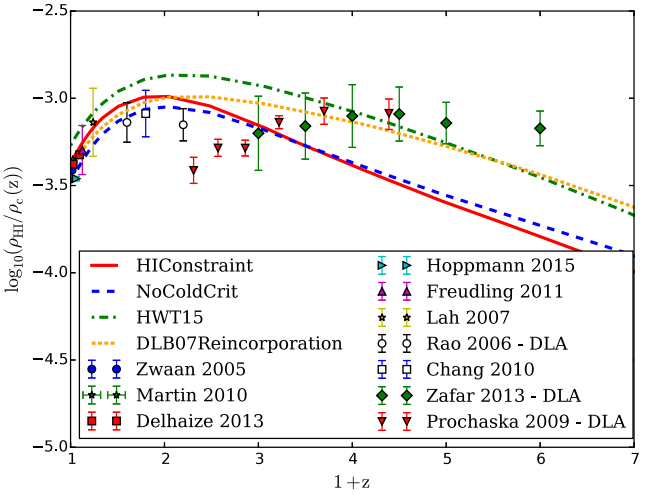

Figure 8. The evolution of the cosmic H I density in units of $\rho_{\rm crit}$. The models are as previously. Plotted in symbols are data from several observational studies. We plot the observations of Zwaan et al. (2005), Martin et al. (2010), Delhaize et al. (2013), Freudling et al. (2011), Hoppmann et al. (2015), Lah et al. (2007), Rao, Turnshek & Nestor (2006), Zafar et al. (2013), Prochaska & Wolfe (2009). The three highest redshift observations come from Damped Lyα observations while below they are from stacking experiments or from direct detections.

amount of star formation (lower-left panel); elsewhere that ratio is similar for all models over all masses. $R_{\rm merge}$ was fixed to 0.1 in all models, slightly compromising the red fraction at $z = 2$, but giving a better match to observed morphologies at $z = 0$ (see HWT15 for further details).

4.2 Star formation

Fig. 6 shows the effect that modifying our models has made to the Kennicutt–Schmidt relation. We include data from four observational data sets – in order to make a fair comparison we have only included literature data that has been averaged over the galactic disc, as in our model. Both the observations and the model of HWT15 show a break in the power-law relation at low surface densities which is not reproduced in the HIConstraint or NoSFThreshold models. The break arises naturally in the HWT15 from the finite threshold surface density for star formation. Although not imposed as a constraint, it seems to arise through a need to prevent galaxies being too blue at $z = 2$. Once we include the H I mass function as a constraint, the break disappears because the improvement in that fit far outweighs the deterioration in the red fraction. We also see a shallower slope which is similar to that observed between H_2 surface density and star formation rate (Bigiel et al. 2008; Wyder et al. 2009). This is perhaps an indicator that we should form stars only out of the H_2 component, although we show in Appendix A below that this does not, of itself, resolve the issues that we see here.

In Fig. 7, we plot the SFRD. All semi-analytic models tend to produce SFRDs that evolve too weakly at low redshift and L-Galaxies is no exception. At $z = 2$ all the models are very similar, while we start seeing more star formation in the new models at lower redshifts. By $z = 0$ there is significantly more star formation in the HIConstraint model than in observations or HWT15.

A more detailed gas division model such as that used in Fu et al. (2010, 2012) may solve the problems presented in this section. Fu et al. (2010, 2012) analysed the impact of different star formation and gas division recipes with spatially-resolved discs producing a match to the observed H I mass function (they still found an excess of dwarfs in the stellar mass function at $z = 2$, but this can likely be solved by the HWT15 gas reincorporation recipe). Spatially-resolved discs have not yet been implemented in the latest version of the Munich model. In order to try to understand the impact of these modifications in our work we have implemented a simplified version of the Fu model. This is described in Appendix A and goes some way to reconciling the Kennicutt–Schmidt relation with the H I mass function. There is therefore some indication that a more realistic gas division along with adjustments to the star formation relation may be the solution.

4.3 Cosmic evolution of H I

In Fig. 8, we plot the evolution of the H I cosmic density, $\Omega_{\rm HI}$. Our results are compared to various observational data sets at different redshifts. The models show more evolution than is found in the

observations, rising to a maximum $\Omega_{\rm HI}$ at $z \approx 1$ before declining at higher redshifts. At this peak, the new models provide a better (but far from perfect) fit to the observations than does HWT15. In future versions of the model there needs to be more H I gas at high redshifts while maintaining the present day values. A similar result was found in Lagos et al. (2014).

4.4 Comparison with other work

Lu14, who also use MCMC techniques to simultaneously fit the H I mass function and the *K*-band luminosity function, obtain much poor fits than we find and claim that generic deficiencies of current SAMs are: (i) extreme mass-loading factors are required in low-mass haloes to expel the H I; (ii) the outflow requires more than 25 per cent of the available supernova energy; and (iii) the star-formation histories of Milky Way sized haloes are far too flat.

We do not require extreme mass-loading factors to achieve an agreement with observations presented in this paper. As shown in fig. S2 of HWT15, the values we assume are comparable to current observational estimates. On the other hand, we do require most of the supernova (SN) energy available to be used to power feedback. However, due to the uncertainties in the amount of energy produced by individual SN events and our neglect of photoionization, we do not believe this rules out the models.

In an attempt to understand the differences in our findings we have undertaken a run using the reincorporation model of De Lucia & Blaizot (2007) which more closely matches that of Lu14. We do not get such a good fit to the H I mass function shown in Fig. 1. As can be seen in the top left panel of Fig. 5, with the DLB07 reincorporation recipe we find we require large mass-loading factors in low-mass galaxies and still don't get a good fit for the H I mass function. This could partially explain the differences between our results and those of Lu14.

Fu et al. (2010, 2012) integrate a model of gas division into a previous version of L-Galaxies, forming stars out of only the H_2 component without using MCMC to constrain the parameters. The model of gas division they use is more complex than that which we implement and the star formation recipe has no dependence on dynamical time. In addition, in regions where the molecular gas dominates the star formation goes as $\Sigma_{\rm SF} \propto \Sigma_{\rm H2}$, while where atomic gas dominates $\Sigma_{\rm SF} \propto \Sigma^2_{\rm gas}$. Their work successfully reproduces the H I mass function. However, as discussed in Section 4.2 they do not reproduce the low-mass end of the stellar mass function as well. Combining the work of Fu with HWT15 in future models of L-Galaxies could provide a solution to simultaneously producing the star-forming properties and the H I mass function. This is hinted at in Appendix A.

Similar work has been undertaken in the Galform model by Lagos et al. (2011a,b) using the same pressure gas division model as used in this work. The gas division was included self-consistently with stars being formed out of the H_2 component. They successfully reproduced the H I mass function but did not reproduce the stellar mass functions as well. Popping, Somerville & Trager (2014), Somerville, Popping & Trager (2015) also implement gas division in their semi-analytic model. They use several models of gas division and star formation and like Lagos et al. (2011a,b) they form stars from the H_2 component. They successfully reproduce several H I observations of galaxies. Their H I mass function exhibits a slight excess at low masses but fits well at the high-mass end. However, their stellar mass function shows significant discrepancies with data at $z = 1$ and 2.

Work has also been done with the Galform model indicating that other forms of feedback, in particular photoionization of atomic gas, could play an important role in the H I content of galaxies (Kim et al. 2013, 2015). This presents an alternative method to suppress the H I in galaxies. In our work we have not explored the effects of new forms of feedback but rather discuss to what extent the H I mass function can be fitted without altering the current model.

5 CONCLUSIONS

In this paper, we have added the H I mass function as an observational constraint to the L-Galaxies semi-analytic model of Henriques et al. (2015). Using MCMC techniques we re-constrain the model parameters in order to best fit this extra observation at $z = 0$ in addition to the stellar mass function and galaxy red fraction at $z = 0$ and $z = 2$. The cold gas content of the model galaxies are divided in post-processing into the H I and H_2 components using the gas division model of Blitz & Rosolowsky (2006) and the approximation to this from Obreschkow et al. (2009).

From this work we conclude:

(i) Using the $z = 0$ H I mass function as an extra constraint we obtain a good fit to this in addition to the stellar mass function and red fraction at $z = 0$ and $z = 2$.

(ii) The most important parameter change is the reduction of the star formation gas surface density threshold. This has been greatly reduced or even removed. This was required to remove the excess of H I gas seen in low-mass galaxies in HWT15. As compensation, the star formation efficiency has decreased, preventing the overproduction of stars in more massive systems.

(iii) The feedback parameters have also changed. The retuned model favours a sharp reduction in the SN ejection efficiency above a halo circular speed of 100 km s^{-1} to much lower efficiencies compared to HWT15. The required mass-loading factors are also reduced slightly compared to HWT15.

(iv) The model has a worse fit to the star formation properties shown in the Kennicutt–Schmidt relation and the cosmic SFRD at low redshifts. We see too much star formation $z = 0$, mostly in the low-mass galaxies. This suggests that we either incorporate and cool too much gas, or that we underestimate the expulsion of gas via winds and stripping. However, since our red fractions roughly agree with observations, any changes must only reduce the star formation efficiency and not halt it completely.

(v) We use the reincorporation model of DLB07 to compare our model with that of Lu14. We alleviate some but not all of the problems identified by Lu14 through using an alternative reincorporation recipe. It is likely that a detailed model gas division and subsequent star formation will be required to match the observations.

Using a more detailed model of cold gas division and a change to the star formation recipe, such as those used in Fu et al. (2010, 2012, 2013), we expect to improve on the problems with simultaneously matching both the star formation properties and the observed H I mass function. In Appendix A we show a simplistic model in which we use the approximation for gas division given in Section 2.2 and then form stars only out of the molecular gas component. While the resulting H I mass function is not as good a fit as our HIConstraint model it is a significant improvement on the original HWT15 fit. Likewise for the Kennicutt–Schmidt relation the model shown in Appendix A is an improvement on the HIConstraint model shown in Fig. 6.

In summary, the cold gas mass function provides a useful constraint on galaxy formation models that poses challenges to the

current paradigm. It is difficult to lower the H I mass function in low-mass galaxies without violating the Kennicutt–Schmidt star formation law and having too much star formation in dwarf galaxies in the current-day Universe. It is likely that a detailed model of the cold gas in the H I and H_2 components and subsequent star formation is required to resolve the issue.

ACKNOWLEDGEMENTS

All authors contributed to the development of the model, the interpretation of the results and the writing of the paper. HM led the bulk of the data analysis and wrote the initial draft of the paper.

The analysis was undertaken on the APOLLO cluster at Sussex. This research made use of ASTROPY, a community-developed core PYTHON package for Astronomy (Robitaille et al. 2013). HM(ORCID 0000-0001-6953-7760) acknowledges the support of her PhD studentship from the Science and Technology Facilities Council (ST/K502364/1). PAT(ORCID 0000-0001-6888-6483) and JL(ORCID 0000-0001-5290-8940) acknowledge support from the Science and Technology Facilities Council (grant number ST/L000652/1). The work of BH(ORCID 0000-0002-1392-489X) was supported by Advanced Grant 246797 'GALFORMOD' from the European Research Council and by a Zwicky Fellowship.

REFERENCES

Angulo R. E., Hilbert S., 2015, MNRAS, 448, 364
Angulo R. E., White S. D. M., 2010, MNRAS, 405, 143
Baldry I. K. et al., 2012, MNRAS, 421, 621
Behroozi P. S., Wechsler R. H., Conroy C., 2013, ApJ, 770, 57
Bell E. F., Mcintosh D. H., Katz N., Weinberg M. D., 2003, ApJS, 149, 289
Benson A. J., 2012, New Astron., 17, 175
Benson A. J., 2014, MNRAS, 444, 2599
Benson A. J., Bower R., 2010, MNRAS, 405, 1573
Bigiel F., Leroy A., Walter F., Brinks E., de Blok W. J. G., Madore B., Thornley M. D., 2008, AJ, 136, 2846
Blitz L., Rosolowsky E., 2006, ApJ, 650, 933 (BR06)
Booth R. S., de Blok W. J. G., Jonas J. L., Fanaroff B., 2009, preprint (arXiv:0910.2935)
Bower R. G., Vernon I., Goldstein M., Benson A. J., Lacey C. G., Baugh C. M., Cole S., Frenk C. S., 2010, MNRAS, 407, 2017
Boylan-Kolchin M., Springel V., White S. D. M., Jenkins A., Lemson G., 2009, MNRAS, 398, 1150
Brown T., Catinella B., Cortese L., Kilborn V., Haynes M. P., Giovanelli R., 2015, MNRAS, 452, 2479
Catinella B. et al., 2013, MNRAS, 436, 34
Cole S., 1991, ApJ, 367, 45
Croton D. J. et al., 2006, MNRAS, 365, 11
Davis T. A. et al., 2014, MNRAS, 444, 3427
De Lucia G., Blaizot J., 2007, MNRAS, 375, 2 (DLB07)
Delhaize J., Meyer M. J., Staveley-Smith L., Boyle B. J., 2013, Detection of H I in distant galaxies using spectral stacking
Domínguez Sánchez H. et al., 2011, MNRAS, 417, 900
Elmegreen B. G., 1989, ApJ, 338, 178
Elmegreen B. G., 1993, ApJ, 411, 170
Freudling W. et al., 2011, ApJ, 727, 40
Fu J., Guo Q., Kauffmann G., Krumholz M. R., 2010, MNRAS, 409, 515
Fu J., Kauffmann G., Li C., Guo Q., 2012, MNRAS, 424, 2701
Fu J. et al., 2013, MNRAS, 434, 16
Giovanelli R. et al., 2005, AJ, 130, 2598
Guo Q. et al., 2011, MNRAS, 413, 101
Guo Q., White S., Angulo R. E., Henriques B., Lemson G., Boylan-Kolchin M., Thomas P., Short C., 2013, MNRAS, 428, 1351
Hatton S., Devriendt J. E. G., Ninin S., Bouchet F. R., Guiderdoni B., Vibert D., 2003, MNRAS, 343, 75
Haynes M. P. et al., 2011, AJ, 142, 170
Henriques B. M. B., Thomas P. A., 2010, MNRAS, 403, 768
Henriques B. M. B., Thomas P. A., Oliver S., Roseboom I., 2009, MNRAS, 396, 535
Henriques B. M. B., White S. D. M., Thomas P. A., Angulo R. E., Guo Q., Lemson G., Springel V., 2013, MNRAS, 431, 3373
Henriques B. M. B., White S. D. M., Thomas P. a., Angulo R., Guo Q., Lemson G., Springel V., Overzier R., 2015, MNRAS, 451, 2663 (HWT15)
Hoppmann L., Staveley-Smith L., Freudling W., Zwaan M. a., Minchin R. F., Calabretta M. R., 2015, MNRAS, 452, 3726
Ilbert O. et al., 2013, A&A, 556, A55
Johnston S. et al., 2008, Exp. Astron., 22, 151
Kampakoglou M., Trotta R., Silk J., 2008, MNRAS, 384, 1414
Kang X., Jing Y. P., Mo H. J., Borner G., 2005, ApJ, 631, 21
Karim A. et al., 2011, ApJ, 730, 61
Kauffmann G., 1996, MNRAS, 281
Kauffmann G., 1999, Am. Astron. Soc. Meet. Abstr., 195
Kauffmann G., White S. D. M., Guiderdoni B., 1993, MNRAS, 264, 201
Kennicutt R. C., 1998, ApJ, 498, 541
Kim H. S., Power C., Baugh C. M., Wyithe J. S. B., Lacey C. G., Lagos C. D. P., Frenk C. S., 2013, MNRAS, 428, 3366
Kim H.-S., Wyithe J. S. B., Power C., Park J., Lagos C. D. P., Baugh C. M., 2015, MNRAS, 453, 2316
Lacey C., Silk J., 1991, ApJ, 381, 14
Lagos C. d. P., Baugh C. M., Lacey C. G., Benson A. J., Kim H.-S., Power C., 2011a, MNRAS, 418, 1649
Lagos C. d. P., Lacey C. G., Baugh C. M., Bower R. G., Benson A. J., 2011b, MNRAS, 416, 1566
Lagos C. D. P., Baugh C. M., Zwaan M. A., Lacey C. G., Gonzalez-Perez V., Power C., Swinbank A. M., van Kampen E., 2014, MNRAS, 440, 920
Lah P. et al., 2007, MNRAS, 376, 1357
Leroy A. K., Walter F., Brinks E., Bigiel F., de Blok W. J. G., Madore B., Thornley M. D., 2008, AJ, 136, 2782
Leroy A. K. et al., 2013, AJ, 146, 19
Li C., White S. D. M., 2009, MNRAS, 398, 12
Lu Y., Mo H. J., Weinberg M. D., Katz N., 2011, MNRAS, 416, 1949
Lu Y., Mo H. J., Katz N., Weinberg M. D., 2012, MNRAS, 421, 1779
Lu Y., Mo H. J., Lu Z., Katz N., Weinberg M. D., 2014, MNRAS, 443, 1252 (Lu14)
Martin A. M., Papastergis E., Giovanelli R., Haynes M. P., Springob C. M., Stierwalt S., 2010, ApJ, 723, 1359
Meyer M. J. et al., 2004, MNRAS, 350, 1195
Mutch S. J., Poole G. B., Croton D. J., 2013, MNRAS, 428, 2001
Muzzin A. et al., 2013, ApJ, 777, 18
Obreschkow D., Croton D., De Lucia G., Khochfar S., Rawlings S., 2009, ApJ, 698, 1467 (O09)
Popping G., Somerville R. S., Trager S. C., 2014, MNRAS, 442, 2398
Prochaska J. X., Wolfe A. M., 2009, ApJ, 696, 1543
Rao S. M., Turnshek D. A., Nestor D. B., 2006, ApJ, 636, 610
Robitaille T. P. et al., 2013, A&A, 558, A33
Ruiz A. N. et al., 2015, ApJ, 801, 139
Schmidt M., 1959, ApJ, 129, 243
Somerville R. S., Primack J. R., 1999, MNRAS, 310, 1087
Somerville R. S., Popping G., Trager S. C., 2015, MNRAS, 453, 4338
Springel V., White S. D. M., Tormen G., Kauffmann G., 2001, MNRAS, 328, 726
Springel V. et al., 2005, Nature, 435, 629
Tomczak A. R. et al., 2014, ApJ, 783, 85
White S. D. M., 1988, NATO Adv. Sci. Institutes Ser. C, 264
White S. D. M., Frenk C. S., 1991, ApJ, 379, 52
Wyder T. K. et al., 2009, ApJ, 696, 1834
Zafar T., Péroux C., Popping A., Milliard B., Deharveng J. M., Frank S., 2013, A&A, 556, A141
Zwaan M. A., Meyer M. J., Staveley-Smith L., Webster R. L., 2005, MNRAS, 359, L30

APPENDIX A: STAR FORMATION FROM MOLECULAR GAS

We have investigated the effect of using the approximation given in equation (7) in order to form stars out of only the H_2 component of the cold gas. The model presented here is not a rigorous exploration of H_2 star formation in the model but rather an attempt to explore if this would provide a solution to some of the problems with our best-fitting model presented here. We modify equation (1) so that the gas mass is that of just the H_2 component and there is no longer any gas density threshold. Here we do not modify the star formation time-scale from equation (1). The resulting H I mass function and Kennicutt–Schmidt relation are shown in Fig. A1 and Fig. A2, respectively. In the H I mass function we see a slight excess of galaxies with low H I masses, significantly better than the original HWT15 but slightly worse than our best-fitting HIConstraint model. The new model roughly fits the slope of Kennicutt–Schmidt relation, although it might not have a sharp enough break at low masses. We conclude that the formation of stars out of only the H_2 component gives an interesting compromise in the comparison between model and observations for the H I mass function and Kennicutt–Schmidt relation. A detailed model of H_2 conversion and subsequent star formation might correct the excessive cold gas in the lowest mass galaxies.

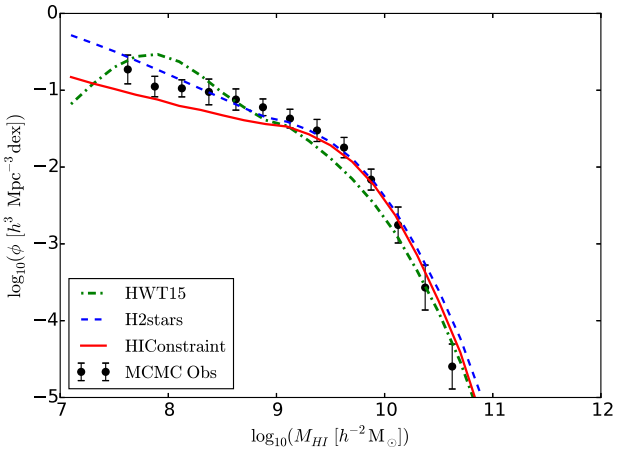

Figure A1. The H I mass function. The red and green lines are as in previous figures; the blue line uses the gas division approximation to form stars out of only H_2 gas.

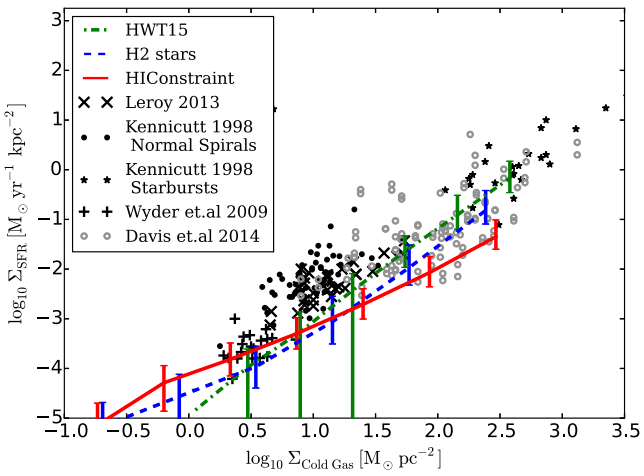

Figure A2. Relationship between total gas surface density and the star formation rate. The contours again enclose 68, 95 and 99 per cent of the data. The red and green are as in previous figures and the blue uses the gas division approximation to form stars out of only H_2 gas. The black data points represent observed values from three different studies (Kennicutt 1998; Wyder et al. 2009; Leroy et al. 2013).

APPENDIX B: COMBINING H I MASS FUNCTION OBSERVATIONS FOR MCMC

We show in Fig. B1 the two data sets used for the H I mass function. These are then combined as described in HWT15 to produce one data set used in the MCMC. The data are combined by averaging the values in the H I mass bin and then the σ is taken to be half the maximum to minimum range. This is a crude method of gauging the statistical error of the combined points and as such we do not quote the formal fits of the model to the data. In Fig. B1 we plot the data from the HIPASS (Zwaan et al. 2005) and ALFALFA (Haynes et al. 2011) along with the combined values used in the MCMC. We choose in this work to only consider the H I mass range present in both observational data sets and so we do not use the lowest masses present in the ALFALFA results alone.

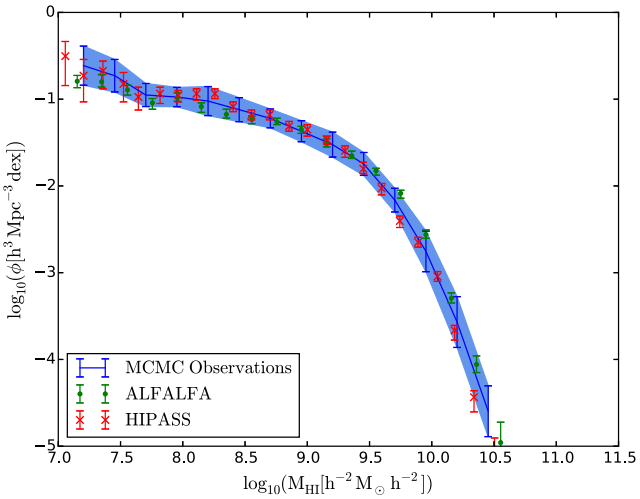

Figure B1. The two data sets combined to form the MCMC observations. The green data is from the ALFALFA survey, Haynes et al. (2011), and the red is from the HIPASS survey, Zwaan et al. (2005). In blue we show the combined data used in the MCMC. The shaded region shows the extent of the errorbars used in the MCMC.

This paper has been typeset from a TEX/LATEX file prepared by the author.